Journal of Applied Physics

RESEARCH ARTICLE | JUNE 25 2025

Energy band alignment in MoS_2/HfO_2: Transfer-related artifacts and interfacial effects

I. Shlyakhov ; K. Iakoubovskii ; D. Lin ; I. Asselberghs ; A. Gaur; G. Delie ; V. Afanas'ev

J. Appl. Phys. 137, 244304 (2025)
https://doi.org/10.1063/5.0279067

Journal of Applied Physics ARTICLE pubs.aip.org/aip/jap

Energy band alignment in MoS_2/HfO_2: Transfer-related artifacts and interfacial effects

Cite as: J. Appl. Phys. **137**, 244304 (2025); doi: 10.1063/5.0279067
Submitted: 5 May 2025 · Accepted: 5 June 2025 ·
Published Online: 25 June 2025

View Online Export Citation CrossMark

I. Shlyakhov,[1,a)] K. Iakoubovskii,[1] D. Lin,[2] I. Asselberghs,[2] A. Gaur,[3] G. Delie,[2] and V. Afanas'ev[2,4]

AFFILIATIONS

[1]Department of Physics, National University of Singapore, Singapore 117542, Singapore
[2]Imec, Kapeldreef 75, Leuven B-3001, Belgium
[3]Robert Bosch GmbH, Reutlingen 72762, Germany
[4]Department of Physics and Astronomy, University of Leuven, Leuven B-3001, Belgium

[a)]**Author to whom correspondence should be addressed:** shlyakhov2017kul@gmail.com

ABSTRACT

The knowledge of energy band alignment in heterojunctions with atomically thin transition metal dichalcogenides (TMDs) is critical for their use in advanced electronic and optoelectronic devices. Despite considerable efforts, the measurement of energy band offset across heterojunctions has been challenging, especially for van der Waals bonded stacks. Key obstacles are related to the scarce and often inconsistent information regarding the bandgap of the TMD layer and the offset between the conduction and valence bands, which is usually inferred from different measurement techniques and samples. To overcome this obstacle, we report combined internal photoemission (IPE) and photoconductivity measurements from 3-monolayer (ML) MoS_2 films, grown by chemical vapor deposition on sapphire and transferred onto HfO_2-covered silicon. We compare the spectral threshold of electron IPE in this heterostructure with IPE data from the Si/HfO_2 interface, yielding the value of the electrostatic potential variation. To improve band offset predictions, we examine the applicability of the classical electron affinity rule by deriving characteristic energies. Our results show that electronic properties at 2D TMD/insulator interfaces depend on the interface processing prior to the 2D material transfer, allowing for the modification of band offsets by adjusting the interface. Furthermore, the measured photoconductivity spectra of 3ML MoS_2 allow us to evaluate the bandgap of the TMD layer, which, combined with the IPE barriers, establishes the interface band diagram of a heterojunction. The presented IPE-based experimental approach can be extended to other two-dimensional TMDs for determining the corresponding band alignment schemes. It evaluates the impact of processing, such as solvent-based MoS_2 transfer, which introduces a dipole and alters band alignment.

I. INTRODUCTION

The emergence of two-dimensional (2D) semiconductors has opened new avenues for next-generation electronic and optoelectronic devices, offering a compelling alternative to conventional silicon technologies.[1,2] With their atomically thin structure, these materials exhibit exceptional electronic and optical properties, making them prime candidates for field-effect transistors,[3–6] spintronic devices,[7,8] and sensor applications.[9] Notably, transition metal dichalcogenides (TMDs) such as MoS_2, $MoSe_2$, WS_2, and WSe_2 stand out owing to their intrinsic semiconducting properties,[10,11] well-defined bandgap that can be tuned by changing the number of layers[10,12] and high charge-carrier mobility.[13,14] A key advantage of these materials lies in their chemically inert surfaces,[15,16] which facilitate ultra-fast charge transport in few-monolayer (ML) thickness range compared to traditional semiconductors such as silicon[17] and indium gallium zinc oxide.[18]

Despite their promising properties, the integration of 2D materials with insulating layers faces critical challenges due to the screening and Coulomb scattering of charge carriers arising from impurities and defects at the interface. For example, empirical studies have demonstrated that amorphous dielectric substrates, such as SiO_2, can significantly reduce charge-carrier mobility in TMDs due to enhanced scattering.[19–23]

Conversely, high-k dielectrics[21,24] and atomically flat 2D insulators like hexagonal boron nitride (hBN) have been shown to

mitigate these effects, leading to superior electrical performance. However, assessing these performance metrics often requires device fabrication, where processing steps can introduce additional nonidealities, complicating direct electrical characterization.[25–27]

An important issue associated with the characterization of TMDs is related to the energy band alignment. In heterojunctions of 2D materials with 3D insulating oxides, electronic transport is influenced by the weak van der Waals (vdW) bonding between them. Crucial parameters that need to be known, and eventually controlled, to enable the fabrication of low-voltage devices, are the energy band offsets for electrons and holes. These offsets are determined by the relative alignment of the energy bands.

Energy band alignment at the interface between 2D materials and insulators is particularly intricate due to the unique nature of these weakly bonded heterostructures. Unlike conventional covalently bonded metal–oxide–semiconductor (MOS) systems, where defect states and interface trap densities can be well characterized, 2D materials introduce additional complexities. For example, SiO_2 is known to host defect bands at 2.6 and 4.6 eV below the conduction band (CB),[28] while HfO_2 possesses defect states approximately 2 eV below the CB.[29] In the case of 2D materials, interfacial species, such as water and hydrocarbons introduced during material transfer or exfoliation, can further influence energy band alignment.[30,31] Additionally, polar hydroxyl (OH) groups on oxide surfaces have been linked to dipole formation and midgap trap states, as observed in transferred MoS_2 layers.[31,32] Unlike traditional high-temperature SiO_2 growth on silicon, which forms a robust covalently bonded interface free of residual contaminants, the van der Waals interaction between 2D materials and insulators inherently permits the persistence of interfacial species, compromising interface passivation and stability.[33]

From a technological standpoint, the use of multilayer 2D semiconductors instead of monolayers (MLs) can offer advantages in mitigating some of these interface-related challenges. Thicker layers exhibit reduced susceptibility to ambient degradation,[34] lower contact resistance due to a smaller bandgap,[35,36] and enhanced current densities. In this study, we investigate the ballistic transport properties of photo-excited electrons across multilayer MoS_2 interfaces with two technologically relevant dielectrics, SiO_2 and HfO_2. Furthermore, we propose a methodology to qualitatively assess band discontinuities at these interfaces, providing insight into optimizing 2D material integration with insulating substrates for device applications.

II. EXPERIMENTAL DETAILS

Large-area (cm^2 scale) 3ML MoS_2 films were synthesized via DC magnetron sputtering of Mo in a sulfur vapor ambient[37] on boron-doped (10^{15} cm^{-3}) (100)-oriented silicon, on which 25 nm oxide was grown by thermal oxidation. The quality of these films, assessed by x-ray photoelectron spectroscopy, Raman scattering, atomic force microscopy (AFM), and other methods, is detailed elsewhere.[38,39]

As an alternative to direct growth on SiO_2/Si, a second series of MoS_2 films were synthesized on c-plane sapphire by metalorganic chemical vapor deposition (MOCVD) with $Mo(CO)_6$, H_2S, H_2, and N_2 precursors at 850 °C and then transferred to HfO_2/TiN/SiO_2/p-Si substrates via a two-step water intercalation process.[40] The average thickness of the MoS_2 film was 2.5 nm that corresponds to three monolayers, as determined by Rutherford backscattering spectrometry and AFM.[41] The target substrate comprised 20 nm of TiN, formed by physical vapor deposition onto 50 nm of SiO_2 that was thermally grown on p-type Si(100). TiN acted as a buried metal gate, decoupling the high-k HfO_2 (12 nm) grown by atomic layer deposition (ALD) using $HfCl_4$ and water precursors from the Si/SiO_2 substrate. Before MoS_2 transfer, the HfO_2 surface was annealed in a forming gas (95:5, N_2:H_2) at 450 °C for 15 min. For internal photoemission (IPE) measurements, both MOS capacitor structures [Fig. 1(a)] had ∼100 nm thick Au pads that are known to form reliable electrical contacts with MoS_2,[42,43] while a blanket Al layer on the silicon wafer's backside served as the back contact.

The Au pads were thermally evaporated through a shadow mask to prevent MoS_2 damage. This measurement geometry allows charge carrier generation studies in monolayer semiconductors beneath 10–20 nm thick semitransparent metal electrodes.[43,44] It further enables detecting the photogeneration of charge carriers in discontinuous semiconductor layers, which is otherwise impossible.

The quantum yield $Y(h\nu)$ of IPE was defined as photocurrent normalized to the incident photon flux and analyzed as a function of photon energy. Photocurrent was measured at room temperature by applying a gate bias V_g and illuminating the sample with monochromatic light from a 150 W Xe arc lamp and Czerny-Turner monochromator. The photocurrent was recorded with a Keithley 6517 A electrometer. The use of Si and MoS_2 electrodes in the same capacitor allows one to use the Si(100) valence band (VB) top edge as reliable energy reference level, enabling the evaluation of conduction band positions in SiO_2, Al_2O_3,[43,45] and HfO_2 insulators with an accuracy of approximately 50–100 meV. The stability of the Si VB across interface conditions stems from minimal dipole or charge effects.[45,46]

To accurately estimate the voltage drop across the insulating oxides, the flatband voltage, corresponding to zero strength of the electric field in the oxide insulator, is determined from IPE current–voltage measurements under illumination with a specific photon energy, at which the photocurrent changes sign. The applied bias, corrected for the flatband voltage, is then divided by the oxide thickness to calculate the average electric field strength. For the 3ML MoS_2/HfO_2/TiN/SiO_2/p-Si stack, the flatband voltage was measured as $V_{fb} = -0.45 \pm 0.1$ V, while for the 3ML MoS_2/SiO_2/p-Si stack structure, it was $V_{fb} = -0.2 \pm 0.1$ V.

III. RESULTS AND DISCUSSION

In MOS capacitors, a 2D TMD film can function as both a light absorber and photo-electron emitter.[12,42,47] Figure 2(a) shows the photocurrent spectrum, plotted in the Powell coordinates $Y^{1/3}(h\nu)$,[48] measured at −1.5 V for the 3ML MoS_2/HfO_2/TiN/SiO_2/p-Si structure. The spectrum features three distinct regions corresponding to different electronic excitation processes. The first region, spanning 1.5–3 eV, is attributed to transient photoconductivity, including the generation of A and B excitons[49] [see the inset in Fig. 2(a)], dissociation, trapping, and carrier collection. Transient photoconductivity is linked to trap states, as evidenced

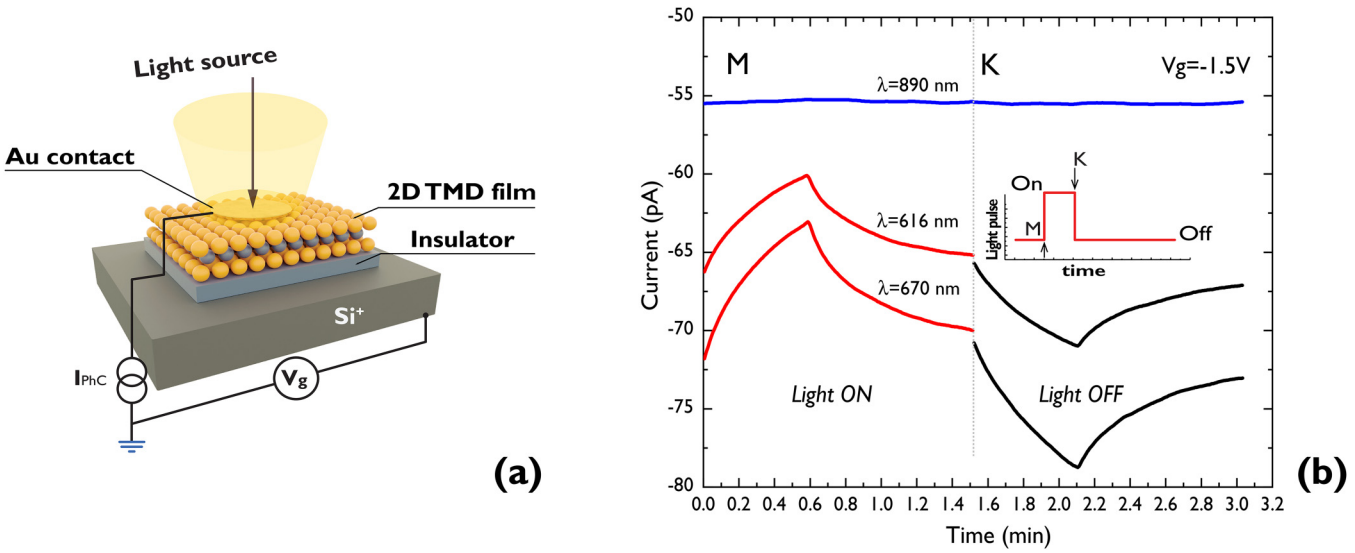

FIG. 1. (a) Schematic of a photocapacitor incorporating a transition metal dichalcogenide (TMD) transferred on top of an insulating layer. (b) The observed relaxation transient of the displacement current in an Au/3ML MoS_2/HfO_2 (12 nm)/TiN/p-type Si structure under a voltage of −1.5 V applied to the 2D layer through an Au contact, illuminated with 616, 670, or 890 nm light. The inset displays the square-shaped light pulse generated by the Xe lamp when the shutter is open. The rising and falling edges of the signal reflect the dynamics of charge trapping at the interface during transitions between illuminated and dark states. The resulting photocurrent arises from carrier transport, followed by the trapping and release (detrapping) of electrons (under negative bias) or holes (under positive bias) at the TMD/insulator interface.

by transient current behavior, observed for short time delays between opening the light shutter and reading the current [Fig. 1(b)]. Upon turning off the light, the trapped carriers are released from oxide traps at the interface, generating a current in the opposite direction and thereby inverting the overall current polarity. Our relaxation current measurements show the dependence of the signal amplitude on the excitation light wavelength [Fig. 1(b)]. Furthermore, when the illumination wavelength is downshifted to 890 nm—below the energy threshold for indirect bandgap transitions in MoS_2—the optical absorption drops dramatically. Consequently, fewer photoexcited carriers are generated, preventing the trap filling and effectively suppressing the observed photocurrent. For photon energies in the range 1.85–2 eV, close to the 3ML indirect gap bandgap, we observe an increase in transient photoconductivity. In contrast, at lower excitation energies (below 1.5 eV), the transient photoconductivity decreases. This indicates the high sensitivity of the measurements to the MoS_2 absorption spectrum.[12]

As photon energy increases, the green curve [(2) in Fig. 2(a)] reveals the IPE of electrons from the MoS_2 VB to the HfO_2 CB. Electrons absorbing photons with energy greater than 3.5 eV can overcome the MoS_2/HfO_2 barrier, contributing to the measured current. At photon energies above 5.5 eV, a further increase in the quantum yield is observed and attributed to intrinsic photoconductivity in the m-phase of HfO_2, i.e., to electron transitions from the oxide VB to the CB as schematically shown in Fig. 2(b). We elaborate this 5.5 eV threshold in Fig. 3, which is discussed below.

Intrinsic photoconductivity in TMDs requires exciton dissociation into free carriers, achieved by applying a DC electric field across the capacitor. The photocurrent is generated by the transport and subsequent trapping or detrapping of electrons at the TMD/insulator interface ($V_g < 0$).[44] Hence, this technique allows us to identify excitonic fingerprints and study photoconductivity in TMDs.

We begin by extracting the IPE spectral thresholds from the yield spectra of 3ML MoS_2 transferred onto HfO_2, as depicted in Fig. 3(a). The $Y^{1/3}(h\nu)$ spectra exhibit a linear relationship within the energy range of 3.6–4.7 eV. This linearity enables the determination of the IPE spectral thresholds, which reflect the energy difference between the top of the MoS_2 VB and the bottom of the HfO_2 CB. The thresholds are identified by extrapolating the IPE yield to zero for each applied bias.

Initial measurements on similar capacitors indicated that the maximum safe applied bias was −2.75 V. Bias values beyond this threshold lead to the breakdown of the insulating layer. With increasing applied bias, the IPE spectra of the 3ML MoS_2 layers develop a tail that extends down to approximately 1.3 eV below the main IPE threshold. This suggests the presence of localized states in the bandgap at the interface or within the oxide layer. It has been confirmed that crystallized HfO_2 films contain deep electron-trapping gap states, which are not eliminated even after annealing at 450 °C. Photo-depopulation spectroscopy on ALD-grown HfO_2 films demonstrates that even after a 15 min anneal at 1000 °C in nitrogen, these trap states remain largely unaffected, indicating their intrinsic nature.[50]

To determine the HfO_2 bandgap, we analyze the photocurrent spectral threshold using the $Y^{1/2}(h\nu)$ plot (Fig. S3 in the supplementary material), which is appropriate for indirect optical

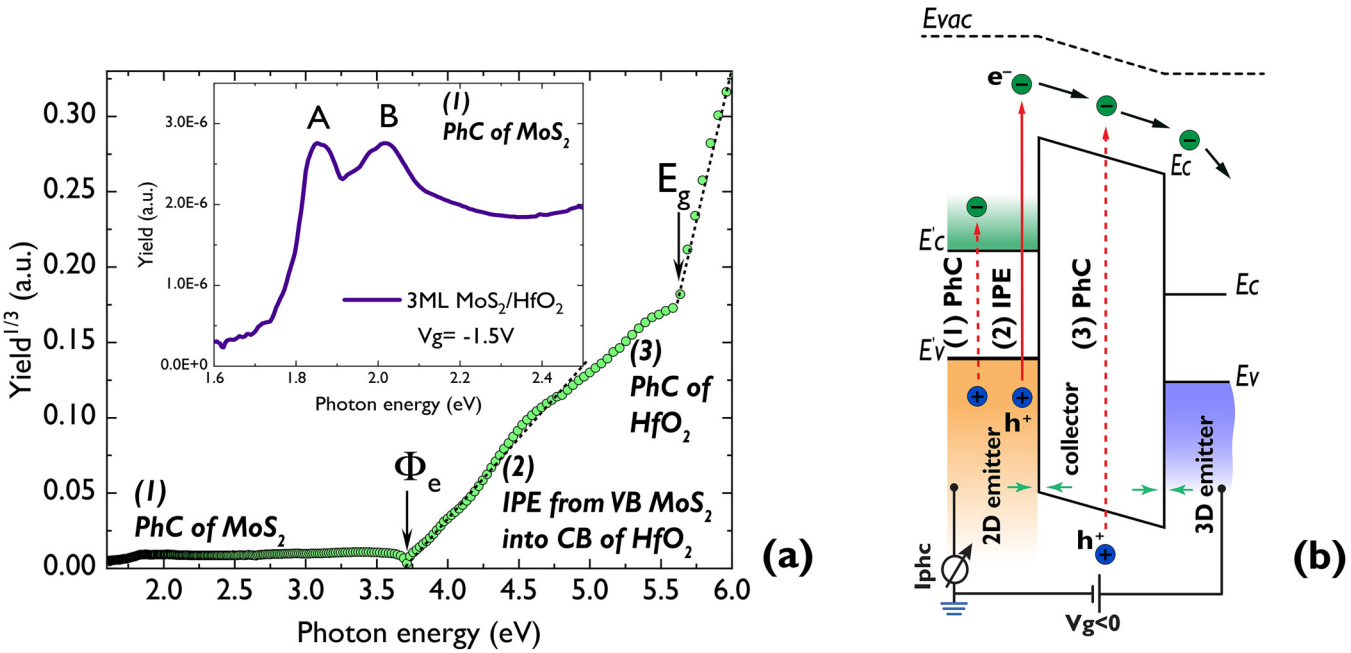

FIG. 2. (a) Cube root of photoemission quantum yield (Y) vs photon energy ($h\nu$) for the 3ML $MoS_2/HfO_2/TiN/SiO_2$/p-Si structure under a −1.5 V bias applied to the top Au electrode. Electrons are injected from the MoS_2 photoemitter into the HfO_2 layer. The spectrum shows several contributions: (1) photoconductivity (PhC) of 3ML MoS_2, (2) internal photoemission (IPE) from the MoS_2 valence band (VB) to the HfO_2 conduction band (CB), and (3) intrinsic photoconductivity of HfO_2. The inset highlights that in the range 1.5–2.5 eV, the measured quantum yield is dominated by the A and B excitons, which dissociate in the applied electric field. (b) Simplified band diagram of the 3ML $MoS_2/HfO_2/TiN/SiO_2$/p-Si capacitor under negative bias ($V_g < 0$). (1) The PhC contribution corresponds to electronic transitions from VB states to the CB of MoS_2. (2) The energy barrier between the MoS_2 VB and the collector CB represents the IPE threshold for electrons. (3) Oxide photoconductivity involves electron excitation to states within the collector's band structure. E_{vac} stands for electron energy in vacuum.

transitions, given that electron crystal momentum is not conserved in optical transitions in amorphous or disordered materials. This inference is consistent with the low dispersion of electron states at the top of the VB of non-magnetic oxides derived from the lone-pair O_{2p} orbitals, which makes the indirect transition model universally applicable to oxide insulators.[47] From the PhC spectra, a threshold is identified by a steep line that marks the band-to-band excitation within the 5.5–6 eV range in the insulator (Fig. S3 in the supplementary material). This allows us to estimate the bandgap as 5.5 eV with an experimental uncertainty of ±0.1 eV. This gap width value is consistent with the presence of the monoclinic m-HfO_2 phase, as established previously through a combination of x-ray diffraction, optical, and photoconductivity measurements.[51,52] The optical transitions at around 5.5 eV across the HfO_2 bandgap indicate a significant degree of crystallization in the HfO_2 layer upon annealing at 450 °C.

To determine the bandgap of the 3ML MoS_2 using the measured displacement photocurrent, we separated the excitonic and free carrier components of the photocurrent and extracted the bandgap of synthetic 3ML MoS_2 films by fitting the spectra to the Tauc model.[12] Figure S2(b) in the supplementary material shows the photocurrent spectra of a 3ML $MoS_2/HfO_2/TiN/SiO_2$/p-Si capacitor, measured at gate voltages of −1 and −1.5 V, normalized to the A exciton peak. An additional B peak at 2.01 eV appears above the A peak. The Tauc plot for the 3ML $MoS_2/HfO_2/TiN/SiO_2$/p-Si capacitor [Fig. 3(b)] was obtained by removing the excitonic component using a linear combination of photocurrent spectra at $V_g = -1$ and −1.5 V. Since the photocurrent I_{phc} is proportional to the absorption coefficient α,[12] the bandgap values can be extracted using the following equation:

$$(I_{phc} \cdot h\nu)^b = C \cdot (h\nu - E_g), \tag{1}$$

where $h\nu$ is the incident photon energy, E_g is the bandgap, C is a constant, and the exponent b equals 2 or 1/2 for the direct or indirect bandgap in a 3D semiconductor, respectively. Then, E_g is extracted by extrapolating the linear region of a $(I_{phc} \times h\nu)^b$ vs $h\nu$ plot to zero current.

This procedure, validated across several capacitors with SiO_2 and HfO_2 insulators and Tauc exponents b = 1/2 and b = 2, yields indirect and direct bandgaps of 1.8 ± 0.1 and 2.4 ± 0.1 eV, respectively. From the Tauc plot and excitonic transition energies, we determine the binding energy of A exciton as $E_{bind} = E_g - E_{exc}$. For 3ML MoS_2, this gives $E_{bind} = 0.55$ eV, consistent with values of 0.3–0.6 eV reported for similar 3ML MoS_2 systems.[12,53]

In multilayer MoS_2, both direct and indirect transitions arise due to its complex band structure. As the number of layers increases,

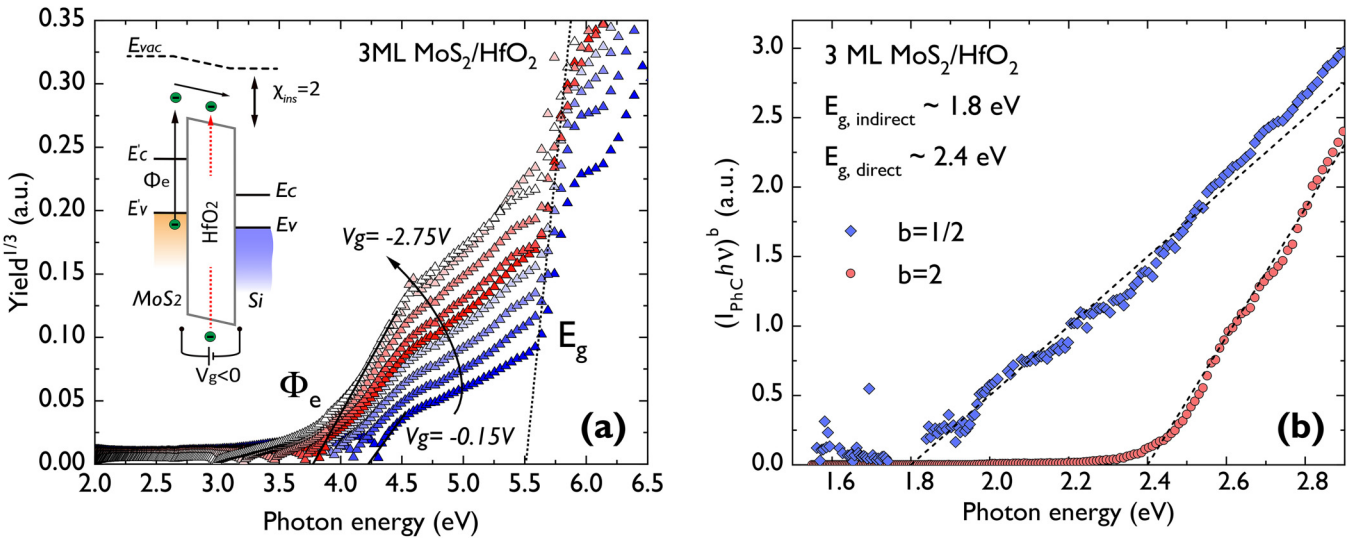

FIG. 3. (a) Cube root of the IPE yield plotted vs photon energy for 3ML MoS_2/m-HfO_2 capacitors under negative biases from −0.15 to −2.75 V. The inset shows a schematic of electronic transitions from the MoS_2 valence band (VB) to the m-HfO_2 conduction band (CB) and its photoconductivity (PhC). The vertical line marks the onset of intrinsic PhC of the oxide with $E_g(HfO_2) = 5.5 \pm 0.1$ eV. (b) Corresponding Tauc plots, where b equals 2 for direct allowed and 1/2 for indirect allowed optical transitions. The extrapolation of the linear region for $b = 1/2$ and $b = 2$ yields 1.8 ± 0.1 and 2.4 ± 0.1 eV for the indirect and direct bandgaps, respectively.

strong spin–orbit coupling and interlayer interactions induce a transition from a direct to an indirect bandgap. Specifically, conduction band splitting along the K–Γ direction in the Brillouin zone lowers the conduction band minimum away from the K point,[54] making indirect transitions energetically favorable. Therefore, for the conduction band offset estimated from IPE, we use the indirect bandgap value of 1.8 eV, as it reflects the dominant excitation pathway and provides a realistic estimate of the carrier injection barrier at the MoS_2/insulator interface. Importantly, the energy barrier extracted from IPE measurements corresponds to the **lowest energy** required for electrons to overcome the interface barrier in the 3ML MoS_2/HfO_2 system. This barrier represents an electronic transition from the global valence band maximum at the Γ point in MoS_2 to conduction band states in the insulator. This is because photoemission is governed by the highest occupied electronic states, and in multilayer MoS_2, the absolute valence band maximum lies at Γ, not at the K point. As a result, transitions involving states at Γ dominate the onset of photoemission, even though the direct transition at K is optically allowed.

The energy of IPE thresholds Φ_e, extracted using the $Y^{1/3}(h\nu)$ plot at different applied voltages for both MoS_2/a-SiO_2 and MoS_2/HfO_2 interfaces, linearly decreases with the square root of electric field F in the oxide [Fig. 3(a)], as expected within the image-force model. This model,[55] also known as the Schottky effect, predicts that $\Phi_e = \Phi_0 - q\sqrt{\frac{qF}{4\pi\varepsilon_0\varepsilon_i}}$, where q is the electron charge, ε_0 is the vacuum dielectric permittivity, and ε_i is the effective image-force constant that corresponds to the dielectric function inside the barrier region and accounts for different polarization processes at the MoS_2/dielectric interface. For the relatively clean 3ML MoS_2/a-SiO_2 interface, where MoS_2 was synthesized under C-free and H-free conditions (slow sputtering of Mo in sulfur vapor), $\varepsilon_i \approx 2$ is close to $\varepsilon_i \approx n^2$, where $n = 1.46$ is the refractive index of SiO_2,[42,45,47] and the IPE barrier height is 3.6 ± 0.05 eV. Combined with experimentally determined indirect gap of 1.8 eV for 3ML MoS_2 and electron affinity of a-SiO_2 $\chi = 0.9$ eV, inferred from the combination of IPE and external photoemission spectral thresholds,[56] this results in a CB offset of ca. 1.85 eV [Fig. 4(b)]. This value closely matches the CB offset derived from the IPE threshold for the 3ML MoS_2/SiO_2 interface,[42,45,47] considering the 1.8 eV bandgap that we determined for 3ML MoS_2 from the Tauc plots of Fig. 3(b). The χ value of 3ML MoS_2, determined using IPE barrier data, the EA of SiO_2, and the bandgap value of 3ML MoS_2, equals 2.7 eV. By contrast, much weaker barrier lowering occurs at the MoS_2/HfO_2 interface with $\varepsilon_i \approx 25$. Such a weak field dependence results in an attenuated image-force interaction between a photoemitted electron and 2D photoemitter. It has been previously observed for MoS_2/a-Al_2O_3 interface[47] and indicates the presence of charge traps at the oxide surface.

The above observation can be further correlated with the corresponding sub-threshold tail in the electron IPE spectra observed for both MoS_2/HfO_2 and MoS_2/a-Al_2O_3 interfaces. As compared to the IPE barrier at the MoS_2/a-SiO_2 interface, a considerably higher IPE threshold of ≈4.1 eV is found for the MoS_2/HfO_2 case [Fig. 4(a)]. The $\chi_{ins}(HfO_2) = 2$ eV value can be estimated using the reported ionization energy of silicon of 5.15 eV[57] and the electron barrier at the Si/HfO_2 interface of 3.1 eV[45,46]—the energy between the top of Si VB and the bottom edge of HfO_2 CB. Taking into account the obtained IPE threshold and the bandgap of 3ML MoS_2, the value of the CB offset at the 3ML MoS_2/HfO_2 interface can be estimated as $E_c = \Phi_e(F) - E_g \approx 2.3$ eV. When combined with the χ value of hafnia, the CB offset results in the electron affinity $\chi \approx 4.3$ eV for 3ML MoS_2.

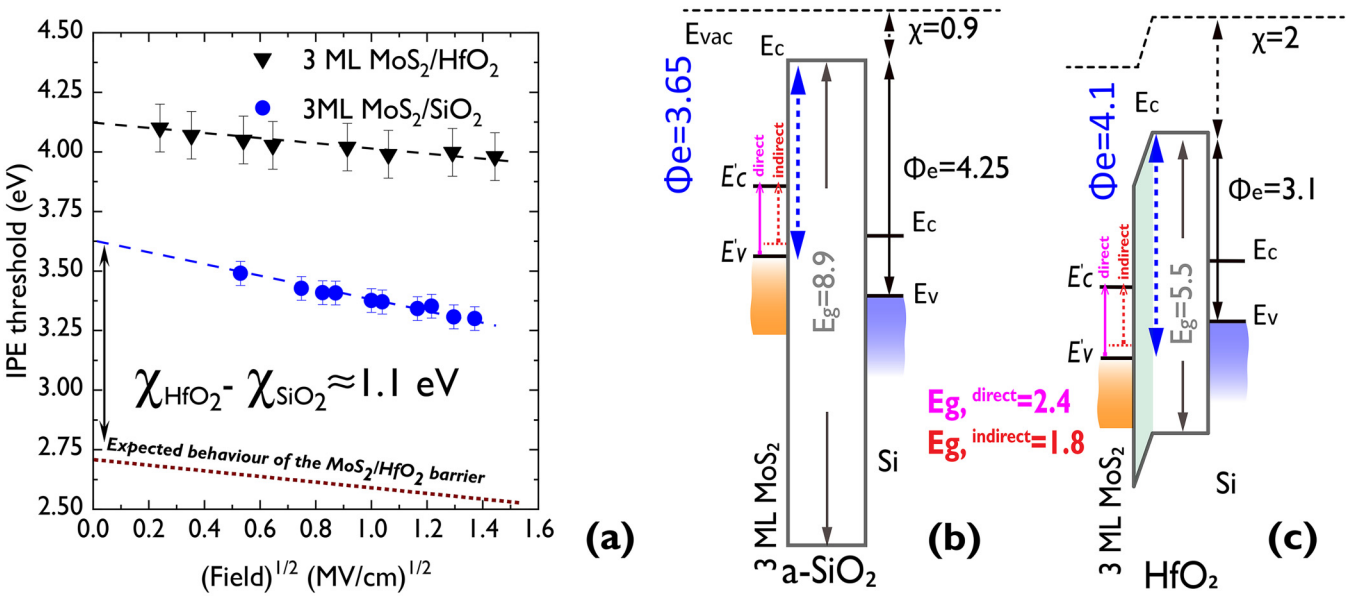

FIG. 4. (a) Schottky plots of the field dependence of the IPE thresholds. Black triangles correspond to an Au/3ML MoS_2/HfO_2 (12 nm)/TiN (20 nm)/a-SiO_2 (50 nm)/p-Si (100) capacitor, while blue circles represent 3ML MoS_2/a-SiO_2 (25 nm)/p-Si (100). Dashed lines show the linear extrapolation to zero field, and the brown dotted line marks the expected VB edge position of 3ML MoS_2 at the m-HfO_2 interface. (b) Band alignments for Si/a-SiO_2/3ML MoS_2 and (c) Si/a-SiO_2/TiN/HfO_2/3ML MoS_2 structures under flatband conditions at the Si/oxide interface, assuming no oxide charges. The measured IPE barriers (Φ_e) and corresponding electron affinities (χ) are shown for each structure. (c) The hypothesized dipole layer at the 3ML MoS_2/HfO_2 interface. All energies are in eV.

Our measurements demonstrate that, contrary to the case of chemically bonded interfaces, the difference in IPE barrier heights for 3ML MoS_2 does not correspond to the difference in the χ values of the insulating films.[45,47,51,56] Note that the difference in the CB offsets, given by $\Delta E_c(\text{Si/a-SiO}_2) - \Delta E_c(\text{Si/HfO}_2) = 1.15$ eV, directly reflects the variation in χ values of the two oxides predicted by the Electron Affinity Rule (EAR). This observation indicates a barrier increase of about 0.6–0.7 eV for the 3ML MoS_2/HfO_2

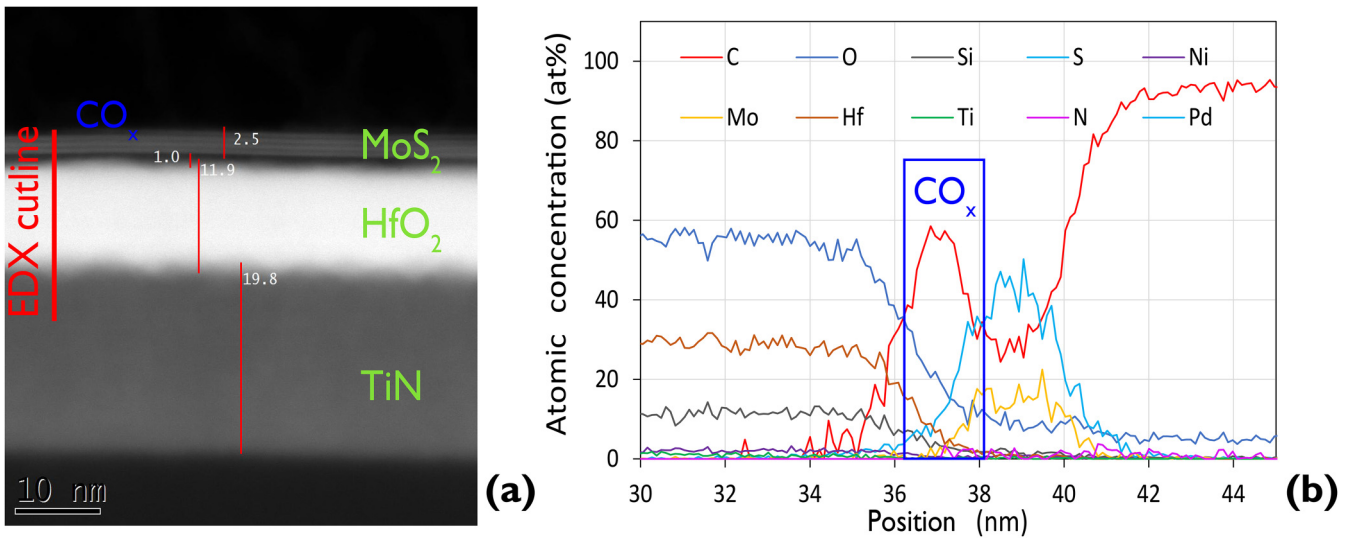

FIG. 5. (a) Cross-sectional TEM micrograph of the TiN/HfO_2/MoS_2 stack showing three complete MLs of MoS_2 with a total thickness of 2.5 nm. A carbon interlayer is seen as a dark contrast at the HfO_2/MoS_2 interface. (b) EDX analysis along the cutline confirms the presence of a 1–2 nm thick carbon-based interlayer.

TABLE I. Summary of the experimental IPE data obtained for the vdW-bonded MoS_2 interfaces as compared to the chemically bonded interfaces with silicon. The Φ_e values correspond to the electron barrier heights between the VB top in the semiconductor and CB bottom in the oxide. IPE experiments revealed no measurable dipole contribution for the MoS_2 films grown in C-free and H-free conditions using magnetron sputtering, as indicated by the "…" symbol. This observation also applies to chemically bonded interfaces. However, surface dipoles with a magnitude of 0.6–1 eV are typically observed for both sulfurization-grown and transferred MoS_2 films. PW stands for the present work.

Interface	Φ_e (eV)	Oxide E_g(eV)	Oxide χ(eV)	$q{\cdot}\Delta$ Vdipole (eV)	Reference
		(1) Van der Waals bonded			
1ML MoS_2/a-SiO_2	4	8.9	0.9	…	45
3ML MoS_2/a-SiO_2	3.6	8.9		…	42
1ML MoS_2/a-Al_2O_3	4.1	6.2	1.9	~1	45
3ML MoS_2/m-HfO_2	4.1	5.5	2	~0.6	PW
		(2) Chemically bonded (bulk)			
Si(100)/a-SiO_2	4.25			…	45
Si(100)/a-Al_2O_3	3.25			…	45
Si(100)/m-HfO_2	3.1			…	46 and 47

heterojunction compared to the EAR prediction. Hence, an additional electrostatic potential variation may be present at the MoS_2/m-HfO_2 interface, which we attribute to an interface dipole layer. Therefore, the EAR needs to be corrected by including the additional term $q\,\Delta$ Vdipole,

$$\Delta Ec = \chi_1 - \chi_2 + q \cdot \Delta \text{Vdipole}, \tag{2}$$

where χ_1 and χ_2 are the χ values of 3ML MoS_2 and HfO_2 layers, and the term $q{\cdot}\Delta$ Vdipole corresponds to an additional drop of approximately 0.7 V in the electrostatic potential across the studied 3ML MoS_2/HfO_2 interface. A possible origin of this dipole is discussed below. It is important to note that a direct comparison of IPE barriers for the two cases—the direct synthesis of 3ML MoS_2 on SiO_2 and the transfer of 3ML MoS_2 onto the HfO_2 (12 nm)/TiN (20 nm)/a-SiO_2(50 nm)/p-Si (100) structure—is not straightforward. This is because, in the latter case, the energy band alignment is influenced by two factors: the intrinsic states at the interface between 3ML MoS_2 and HfO_2 (12 nm), as well as potential interface contamination resulting from the MoS_2 transfer.

To better understand the possible origin of the observed IPE barrier increase as a result of TMD layer transfer and indicate possible factors disturbing the electrostatic potential distribution across the MoS_2/HfO_2 interface, cross-sectional transmission electron microscopy (TEM) and energy-dispersive x-ray spectroscopy (EDX) analysis was performed (Fig. 5). TEM and EDX analysis of the investigated MoS_2/HfO_2/TiN/SiO_2/p-Si stack revealed the presence of a ca. 1–2 nm thick carbon-rich interlayer, probably resulting from the wet transfer processing and the use of a polymethyl methacrylate protective layer during processing. This is in stark contrast to the interface quality observed when few-ML MoS_2 was directly grown on SiO_2 by DC magnetron sputtering of Mo in sulfur vapor (Mo + S process) without the MoS_2 layer transfer (Fig. S4 in the supplementary material). Hence, the behavior of the IPE threshold at MoS_2/HfO_2 interface and the observed failure of the EAR due to the electroneutrality violation may be explained by the incorporation of carbon residuals and water interaction with the oxide surface as a result of MoS_2 layer transfer. It suggests that the carbon residuals along with the interstitial water molecules and the surface hydroxyl (O–H) groups are the potential factors to account for the observed electroneutrality violation, which is detrimental to e electrostatics of the van der Waals bonded MoS_2/oxide interfaces.

Using the inferred IPE barriers Φ_e measured for the van der Waals bonded interfaces between 2D TMD and three different insulating oxides, and for the chemically bonded bulk interfaces, i.e., the 3ML MoS_2/a-SiO_2 vs the Si/a-SiO_2 case, the 3ML MoS_2/HfO_2 vs the Si/HfO_2 interface, etc., we constructed the band alignment schematics shown in Figs. 4(b) and 4(c). The value of the IPE barrier measured at the Si/HfO_2 interface and the Si bandgap are either taken from the literature[45,46,55,58] or measured in the present work. As can be seen from Fig. 4, the barriers at the Si/a-SiO_2 and Si/HfO_2 interfaces are sensitive to changes in χ values of the oxide insulator, and, therefore, the EAR remains pertinent for these 3D chemically bonded heterojunctions. By contrast, the ideal affinity rule fails for both the MoS_2/a-Al_2O_3 and the MoS_2/HfO_2 interfaces by predicting significantly lower barriers than the experimentally observed ones. IPE data are summarized in Table I.

IV. CONCLUSIONS

Analysis of 3ML MoS_2 interfaces with a-SiO_2 and HfO_2 reveals a deviation from the expected ideal Schottky–Mott scenario when 3ML MoS_2 is transferred onto HfO_2. This deviation is primarily attributed to violations of interface electroneutrality, stemming from chemical modification of the oxide surface and the presence of a ca. 1 nm interlayer that contains carbon polymer and water residues from the 2D layer transfer process. Such interfacial contaminations can significantly affect the performance of TMD-based transistors, as they may lead to increased carrier scattering and the threshold voltage shift. Furthermore, the presence of these contaminants introduces electron states accessible for charge carriers in the TMD layer raising reliability concerns due to charge trapping. The IPE data indicate the existence of a polarization layer with a net negative

charge that results in an electrostatic potential variation of approximately 0.7 V across the interface. Our findings demonstrate that band alignment at 2D TMD/insulator interfaces is not only determined by the intrinsic properties of the 2D materials but is significantly affected by interfacial chemistry and processing conditions, which particularly affects the insulating oxide surface. The Schottky–Mott model and electron affinity rule are insufficient for describing these interfaces, highlighting the necessity for interface barrier height monitoring to enable interfacial engineering to control the band offsets and built-in potentials. Processing improvements, such as enhanced surface cleaning and dry transfer techniques, are essential for reducing interface contamination.

SUPPLEMENTARY MATERIAL

See the supplementary material for photoconductivity measurements and bandgap determination.

ACKNOWLEDGMENTS

The work at KULeuven received partial support from Flanders Innovation & Entrepreneurship [2Dfun (2D functional MX2/graphene hetero-structures), an ERA-NET project in the framework of the EU Graphene Flagship], and from KU Leuven Internal Fund (Project No. C14/16/061).

AUTHOR DECLARATIONS

Conflict of Interest

The authors have no conflicts to disclose.

Author Contributions

I. Shlyakhov: Conceptualization (lead); Data curation (lead); Formal analysis (lead); Investigation (lead); Methodology (lead); Writing – original draft (lead); Writing – review & editing (lead). **K. Iakoubovskii:** Conceptualization (equal); Methodology (equal); Writing – review & editing (equal). **D. Lin:** Conceptualization (equal); Methodology (equal). **I. Asselberghs:** Supervision (supporting). **A. Gaur:** Investigation (supporting). **G. Delie:** Investigation (supporting). **V. Afanas'ev** Conceptualization (equal); Project administration (lead); Supervision (lead); Writing – review & editing (equal).

DATA AVAILABILITY

The data that support the findings of this study are available from the corresponding author upon reasonable request.

REFERENCES

[1]Y. Yoon, K. Ganapathi, and S. Salahuddin, "How good can monolayer MoS_2 transistors be," Nano Lett. **11**, 3768–3773 (2011).
[2]K. S. Novoselov, D. Jiang, F. Schedin, T. J. Booth, V. V. Khotkevich, S. V. Morozov, and A. K. Geim, "Two-dimensional atomic crystals," Proc. Natl. Acad. Sci. U.S.A. **102**, 10451–10453 (2005).
[3]V. Podzorov, M. E. Gershenson, C. Kloc, R. Zeis, and E. Bucher, "High-mobility field-effect transistors based on transition metal dichalcogenides," Appl. Phys. Lett. **84**, 3301–3303 (2004).
[4]B. Radisavljevic, A. Radenovic, J. Brivio, V. Giacometti, and A. Kis, "Single-layer MoS_2 transistors," Nat. Nanotechnol. **6**, 147–150 (2011).
[5]H. J. Chuang, X. Tan, N. J. Ghimire, M. M. Perera, B. Chamlagain, M. M. C. Cheng, J. Yan, D. Mandrus, D. Tománek, and Z. Zhou, "High mobility WSe_2 p- and n-type field-effect transistors contacted by highly doped graphene for low-resistance contacts," Nano Lett. **14**, 3594–3601 (2014).
[6]J. Pu, Y. Yomogida, K. K. Liu, L. J. Li, Y. Iwasa, and T. Takenobu, "Highly flexible MoS_2 thin-film transistors with ion gel dielectrics," Nano Lett. **12**, 4013–4017 (2012).
[7]X. Xu, W. Yao, D. Xiao, and T. F. Heinz, "Spin and pseudospins in layered transition metal dichalcogenides," Nat. Phys. **10**(5), 343 (2014).
[8]S. Wu, J. S. Ross, G. B. Liu, G. Aivazian, A. Jones, Z. Fei, W. Zhu, D. Xiao, W. Yao, D. Cobden, and X. Xu, "Electrical tuning of valley magnetic moment through symmetry control in bilayer MoS_2," Nat. Phys. **9**, 149–153 (2013).
[9]G. Eda and S. A. Maier, "Two-dimensional crystals: Managing light for optoelectronics," ACS Nano **7**, 5660–5665 (2013).
[10]K. C. Santosh, R. C. Longo, R. Addou, R. M. Wallace, and K. Cho, "Impact of intrinsic atomic defects on the electronic structure of MoS_2 monolayers," Nanotechnology **25**, 375703 (2014).
[11]K. F. Mak, C. Lee, J. Hone, J. Shan, and T. F. Heinz, "Atomically thin MoS_2: A new direct-gap semiconductor," Phys. Rev. Lett. **105**, 136805 (2010).
[12]I. Shlyakhov, K. Iakoubovskii, S. Banerjee, A. Gaur, D. Lin, I. Asselberghs, I. Radu, J. Chai, M. Yang, S. J. Wang, M. Houssa, A. Stesmans, and V. Afanas'ev, "Measurement of direct and indirect bandgaps in synthetic ultrathin MoS_2 and WS_2 films from photoconductivity spectra," J. Appl. Phys. **129**, 155302 (2021).
[13]S. Kim, A. Konar, W. S. Hwang, J. H. Lee, J. Lee, J. Yang, C. Jung, H. Kim, J.-B. Yoo, J.-Y. Choi, Y. W. Jin, S. Y. Lee, D. Jena, W. Choi, and K. Kim, "High-mobility and low-power thin-film transistors based on multilayer MoS_2 crystals," Nat. Commun. **3**, 1011 (2012).
[14]F. Reale, P. Palczynski, I. Amit, G. F. Jones, J. D. Mehew, A. Bacon, N. Ni, P. C. Sherrell, S. Agnoli, M. F. Craciun, S. Russo, and C. Mattevi, "High-mobility and high-optical quality atomically thin WS_2," Sci. Rep. **7**, 14911 (2017).
[15]B. Chen, H. Sahin, A. Suslu, L. Ding, M. I. Bertoni, F. M. Peeters, and S. Tongay, "Environmental changes in $MoTe_2$ excitonic dynamics by defects-activated molecular interaction," ACS Nano **9**, 5326 (2015).
[16]P. J. Wyndaele, J. F. de Marneffe, R. Slaets, B. Groven, A. Franquet, P. Brüner, T. Grehl, and S. De Gendt, "2D TMDC aging: A case study of monolayer WS_2 and mitigation strategies," Nanotechnology **35**, 475702 (2024).
[17]Y. Liu, X. Duan, H. J. Shin, S. Park, Y. Huang, and X. Duan, "Promises and prospects of two-dimensional transistors," Nature **591**, 43–53 (2021).
[18]J. H. Jeong, S. W. Seo, D. Kim, S. H. Yoon, S. H. Lee, B. J. Kuh, and J. K. Jeong, "Specific contact resistivity reduction in amorphous IGZO thin-film transistors through a TiN/IGTO heterogeneous interlayer," Sci. Rep. **14**, 10953 (2024).
[19]D. Rhodes, S. H. Chae, R. Ribeiro-Palau, and J. Hone, "Disorder in van der Waals heterostructures of 2D materials," Nat. Mater. **18**(6), 541–549 (2019).
[20]Y. Y. Illarionov, G. Rzepa, M. Waltl, T. Knobloch, A. Grill, M. M. Furchi, T. Mueller, and T. Grasser, "The role of charge trapping in MoS_2/SiO_2 and MoS_2/hBN field-effect transistors," 2D Mater. **3**(3), 035004 (2016).
[21]L. Banszerus, M. Schmitz, S. Engels, J. Dauber, M. Oellers, F. Haupt, K. Watanabe, T. Taniguchi, B. Beschoten, and C. Stampfer, "Ultrahigh-mobility graphene devices from chemical vapor deposition on reusable copper," Sci. Adv. **1**, e1500222 (2015).
[22]Q. A. Vu, S. Fan, S. H. Lee, M. K. Joo, W. J. Yu, and Y. H. Lee, "Near-zero hysteresis and near-ideal subthreshold swing in h-BN encapsulated single-layer MoS_2 field-effect transistors," 2D Mater. **5**, 031001 (2018).
[23]N. Huo, Y. Yang, Y. N. Wu, X. G. Zhang, S. T. Pantelides, and G. Konstantatos, "High carrier mobility in monolayer CVD-grown MoS_2 through phonon suppression," Nanoscale **10**(31), 15071–15077 (2018).
[24]M. D. Tran, J. H. Kim, H. Kim, M. H. Doan, D. L. Duong, and Y. H. Lee, "Role of hole trap sites in MoS_2 for inconsistency in optical and electrical phenomena," ACS Appl. Mater. Interfaces **10**, 10580 (2018).

[25]A. Leonhardt, D. Chiappe, I. Asselberghs, C. Huyghebaert, I. Radu, and S. De Gendt, "Improving MOCVD MoS_2 electrical performance: Impact of minimized water and air exposure conditions," IEEE Electron Device Lett. **38**, 1606–1609 (2017).
[26]Y. Liu, J. Guo, E. Zhu, L. Liao, S. J. Lee, M. Ding, I. Shakir, V. Gambin, Y. Huang, and X. Duan, "Approaching the Schottky–Mott limit in van der Waals metal–semiconductor junctions," Nature **557**(7707), 696–700 (2018).
[27]C. M. Smyth, R. Addou, S. McDonnell, C. L. Hinkle, and R. M. Wallace, "Contact metal–MoS_2 interfacial reactions and potential implications on MoS_2-based device performance," J. Phys. Chem. C **120**(27), 14719–14729 (2016).
[28]Y. Y. Illarionov, A. G. Banshchikov, D. K. Polyushkin, S. Wachter, T. Knobloch, M. Thesberg, L. Mennel, M. Paur, M. Stöger-Pollach, A. Steiger-Thirsfeld, M. I. Vexler, M. Waltl, N. S. Sokolov, T. Mueller, and T. Grasser, "Ultrathin calcium fluoride insulators for two-dimensional field-effect transistors," Nat. Electron. **2**, 230 (2019).
[29]F. Cerbu, O. Madia, D. V. Andreev, S. Fadida, M. Eizenberg, L. Breuil, J. G. Lisoni, J. A. Kittl, J. Strand, A. L. Shluger, V. V. Afanas'ev, M. Houssa, and A. Stesmans, "Intrinsic electron traps in atomic-layer deposited HfO_2 insulators," Appl. Phys. Lett. **108**(22), 222901 (2016).
[30]V. V. Afanas'ev, D. Chiappe, A. Leonhardt, M. Houssa, C. Huyghebaert, I. Radu, and A. Stesmans, "(Invited) internal photoemission of electrons from 2-dimensional semiconductors," ECS Trans. **80**, 191–201 (2017).
[31]V. V. Afanas'ev, D. Chiappe, M. Perucchini, M. Houssa, C. Huyghebaert, I. Radu, and A. Stesmans, "Impact of MoS_2 layer transfer on electrostatics of MoS_2/SiO_2 interface," Nanotechnology **30**, 055702 (2019).
[32]B. Schoenaers, A. Leonhardt, A. Nalin Mehta, A. Stesmans, D. Chiappe, I. Asselberghs, I. Radu, C. Huyghebaert, S. De Gendt, M. Houssa, and V. V. Afanas'ev, "Analysis of transferred MoS_2 layers grown by MOCVD: Evidence of Mo vacancy related defect formation," ECS J. Solid State Sci. Technol. **9**(9), 093001 (2020).
[33]L. T. Zhuravlev, "The surface chemistry of amorphous silica. Zhuravlev model," Colloids Surf. A **173**, 1–38 (2000).
[34]H. Qiu, L. Pan, Z. Yao, J. Li, Y. Shi, and X. Wang, "Electrical characterization of back-gated bi-layer MoS_2 field-effect transistors and the effect of ambient on their performances," Appl. Phys. Lett. **100**, 123104 (2012).
[35]H. Zhong, R. Quhe, Y. Wang, Z. Ni, M. Ye, Z. Song, Y. Pan, J. Yang, L. Yang, M. Lei, J. Shi, and J. Lu, "Interfacial properties of monolayer and bilayer MoS_2 contacts with metals: Beyond the energy band calculations," Sci. Rep. **6**, 21786 (2016).
[36]J. Kwon, J. Y. Lee, Y. J. Yu, C. H. Lee, X. Cui, J. Hone, and G. H. Lee, "Thickness-dependent Schottky barrier height of MoS_2 field-effect transistors," Nanoscale **9**, 6151–6157 (2017).
[37]J. Tao, J. W. Chai, Z. Zhang, J. S. Pan, and S. J. Wang, "The energy-band alignment at molybdenum disulphide and high-k dielectrics interfaces," Appl. Phys. Lett. **104**, 232110 (2014).
[38]J. Tao, J. Chai, X. Lu, L. M. Wong, T. I. Wong, J. Pan, Q. Xiong, D. Chi, and S. Wang, "Growth of wafer-scale MoS_2 monolayer by magnetron sputtering," Nanoscale **7**, 2497–2503 (2015).
[39]Z. P. Ling, R. Yang, J. W. Chai, S. J. Wang, W. S. Leong, Y. Tong, D. Lei, Q. Zhou, X. Gong, D. Z. Chi, and K. W. Ang, "Large-scale two-dimensional MoS_2 photodetectors by magnetron sputtering," Opt. Express **23**, 13580 (2015).
[40]D. Chiappe, J. Ludwig, A. Leonhardt, S. El Kazzi, A. Nalin Mehta, T. Nuytten, U. Celano, S. Sutar, G. Pourtois, M. Caymax, K. Paredis, W. Vandervorst, D. Lin, S. De Gendt, K. Barla, C. Huyghebaert, I. Asselberghs, and I. Radu, "Layer-controlled epitaxy of 2D semiconductors: Bridging nanoscale phenomena to wafer-scale uniformity," Nanotechnology **29**(42), 425602 (2018).
[41]Q. Smets, G. Arutchelvan, J. Jussot, D. Verreck, I. Asselberghs, A. N. Mehta, and I. Radu, "Ultra-scaled MOCVD MoS_2 MOSFETs with 42 nm contact pitch and 250μA/μm drain current," in *IEEE International Electron Devices Meeting (IEDM)* (IEEE, 2019), pp. 23.2.1–23.2.4.
[42]I. Shlyakhov, J. Chai, M. Yang, S. J. Wang, V. V. Afanas'ev, M. Houssa, and A. Stesmans, "Band alignment at interfaces of synthetic few-monolayer MoS_2 with SiO_2 from internal photoemission," APL Mater. **6**, 026801 (2018).
[43]I. Shlyakhov, S. Achra, N. Bosman, I. Asselberghs, C. Huyghebaert, I. Radu, J. Chai, M. Yang, S. J. Wang, A. Bol, K. Iakoubovskii, M. Houssa, A. Stesmans, and V. V. Afanas'ev, "Internal photoemission of electrons from 2D semiconductor/3D metal barrier structures," J. Phys. D: Appl. Phys. **54**(29), 295101 (2021).
[44]V. V. Afanas'ev, J. Schubert, A. Neft, G. Delie, I. Shlyakhov, V. Trepalin, M. Houssa, and A. Stesmans, "Determination of energy thresholds of electron excitations at semiconductor/insulator interfaces using trap-related displacement currents," Microelectron. Eng. **215**, 110992 (2019).
[45]V. V. Afanas'ev, *Internal Photoemission Spectroscopy* (Elsevier, 2014), pp. 1–404.
[46]V. V. Afanas'ev and A. Stesmans, "Internal photoemission at interfaces of high-k insulators with semiconductors and metals," J. Appl. Phys. **102**(8), 081301 (2007).
[47]I. Shlyakhov, J. Chai, M. Yang, S. Wang, V. V. Afanas'ev, M. Houssa, and A. Stesmans, "Energy band alignment of a monolayer MoS_2 with SiO_2 and Al_2O_3 insulators from internal photoemission," Phys. Status Solidi A **216**, 1800616 (2019).
[48]R. Powell, "Interface barrier energy determination from voltage dependence of photoinjected currents.," J. Appl. Phys. **41**, 2424–2432 (1970).
[49]S. Golovynskyi, I. Irfan, M. Bosi, L. Seravalli, O. I. Datsenko, I. Golovynska, and J. Qu, "Exciton and trion in few-layer MoS_2: Thickness- and temperature-dependent photoluminescence," Appl. Surf. Sci. **515**, 146033 (2020).
[50]J. Strand, M. Kaviani, D. Gao, A. M. El-Sayed, V. V. Afanas'ev, and A. L. Shluger, "Intrinsic charge trapping in amorphous oxide films: Status and challenges," J. Phys.: Condens. Matter **30**, 233001 (2018).
[51]E. E. Hoppe, R. S. Sorbello, and C. R. Aita, "Near-edge optical absorption behavior of sputter deposited hafnium dioxide," J. Appl. Phys. **101**, 123534 (2007).
[52]L. Pantisano, V. V. Afanas'Ev, S. Cimino, C. Adelmann, L. Goux, Y. Y. Chen, J. A. Kittl, D. Wouters, and M. Jurczak, "Towards barrier height modulation in HfO_2/TiN by oxygen scavenging—Dielectric defects or metal induced gap states?," Microelectron. Eng. **88**, 1251–1254 (2011).
[53]E. V. Shornikova, D. R. Yakovlev, N. A. Gippius, G. Qiang, B. Dubertret, A. H. Khan, A. Di Giacomo, I. Moreels, and M. Bayer, "Exciton binding energy in CdSe nanoplatelets measured by one- and two-photon absorption," Nano Lett. **21**(24), 10525 (2021).
[54]J. E. Padilha, H. Peelaers, A. Janotti, and C. G. Van de Walle, "Nature and evolution of the band-edge states in MoS_2: From monolayer to bulk," Phys. Rev. B **90**, 205420 (2014).
[55]V. K. Adamchuk and V. V. Afanas'ev, "Internal photoemission spectroscopy of semiconductor-insulator interfaces," Prog. Surf. Sci. **41**, 111–211 (1992).
[56]R. Williams, "Photoemission of electrons from silicon into silicon dioxide. Effects of ion migration in the oxide," J. Appl. Phys. **37**, 1491–1494 (1966).
[57]F. G. Allen and G. W. Gobeli, "Energy structure in photoelectric emission from Cs-covered silicon and germanium," Phys. Rev. **144**, 558–575 (1966).
[58]S. Sze, *Physics of Semiconductor Devices* (Wiley-Interscience Publication, John Wiley & Sons, 1981).